Spin alignment of vector mesons by second-order hydrodynamic gradients

Avdhesh Kumar[*] and Di-Lun Yang[†]
Institute of Physics, Academia Sinica, Taipei, 11529, Taiwan

Philipp Gubler[‡]
Advanced Science Research Center, Japan Atomic Energy Agency, Tokai, Ibaraki 319-1195, Japan

(Received 5 January 2024; accepted 25 February 2024; published 27 March 2024)

Starting with the polarization dependent Wigner function of vector mesons, we derive an expression for the 00–component (ρ_{00}) of spin density matrix in terms of the second order gradients of the vector meson distribution functions. We further apply a thermal model to analyze the transverse momentum and the azimuthal angle dependence of ρ_{00} for ϕ and K^{*0} mesons resulting from distribution gradients in Au-Au collisions with $\sqrt{s_{NN}} = 130$ GeV at midrapidity. Our results for the transverse momentum dependence indicate that the deviations of ρ_{00} from $1/3$ as the signal for spin alignment are greatly enhanced at large transverse momenta and have a strong centrality dependence while analysis of the azimuthal angle (ϕ_q) dependence suggest that such deviations have a $\cos(2\phi_q)$ structure with opposite sign for ϕ and K^{*0}. Our finding may be considered as a baseline for probing spin-alignment mechanisms beyond hydrodynamic gradients.

DOI: 10.1103/PhysRevD.109.054038

I. INTRODUCTION

Strongly interacting matter created in noncentral collisions of two heavy nuclei at relativistic beam energies carries a huge amount of global orbital angular momentum along the direction perpendicular to the reaction plane. A fraction of such orbital angular momentum can get transferred into the spin degrees of freedom which in turn may lead to the spin polarization of emitted particles [1–7] in a way similar to the Barnett effect [8] and the Einstein–de Haas effect [9] in materials. As a matter of fact, a nonzero global and local spin polarization of hyperons has been measured by the STAR Collaboration [10–13] at BNL, the ALICE Collaboration at CERN [14], and the HADES Collaboration at GSI [15]. Theoretically, relativistic hydrodynamics that makes use of the global thermodynamic equilibrium formula, which connects the mean spin pseudovector of a fermion with the thermal vorticity [16–20], turned out be a successful tool in describing the experimentally measured global polarization of Λ-hyperons [18,19,21–25]. Surprisingly, the predictions for the *local* spin polarization, i. e. the momentum dependence of the longitudinal spin polarization [19,26], fails to agree with the measured values [11]. This result has motivated further theoretical developments, trying to clarify the origins of spin polarization and spin transport phenomena in relativistic heavy ion collisions [27–53] (see Refs. [54,55] for recent reviews). Such developments include investigating the roles of the symmetric gradients of hydrodynamic variables (known as thermal shear) [27,29,30], gradients of chemical potentials [27,28] and spin potentials [35]. Interestingly, taking into account thermal shear corrections in local equilibrium, theoretical results for the local spin polarization of Λ hyperons agree with the experimental data only if the effect of temperature gradients are neglected [56] or the Λ hyperon mass is replaced with its constituent strange quark mass [57,58].

Unlike hyperons, vector mesons decay via strong or electromagnetic interactions in which parity is conserved. Therefore, the spin polarization of vector mesons cannot be measured directly as the direction of polarization is not known. However, the spin alignment of vector mesons can be studied by measuring the deviations from the equilibrium value ($1/3$) of ρ_{00}, which parametrizes the only independent degree of freedom among the three diagonal elements (ρ_{00}, ρ_{11}, $\rho_{-1,-1}$) of the 3×3 Hermitian spin density matrix with unit trace, assuming that parity is conserved [59,60]. Experimental measurements [61–64] indicate that the global spin alignment of vector mesons is much larger than theoretical predictions based on the assumption of thermal equilibrium [6,65] and the spin coalescence model [1,66]. Furthermore, both quantitative and qualitative differences exist between distinct flavors and different collision energies [61–64]. For example, at LHC energies, $\rho_{00} < 1/3$ is observed for both ϕ and K^{*0} mesons with small transverse momenta [61] while at RHIC energies, $\rho_{00} > 1/3$ for ϕ and

[*]avdheshk@gate.sinica.edu.tw
[†]dlyang@gate.sinica.edu.tw
[‡]philipp.gubler1@gmail.com

$\rho_{00} \approx 1/3$ for K^{*0} were globally found [64] (see also Ref. [62] for some experimental results of J/ψ spin alignments). Such results have motivated the development of various theoretical mechanisms [67–83] but the issue remains unresolved. We note especially that the treatment of hydrodynamic gradients in this context has so far been incomplete. Specifically, only a negligible contribution from such gradients was estimated based on the small spin polarization from the vorticity of strange quarks in the coalescence model (see e.g. [69]). A similar result is expected based on the shear-induced polarization (governed by the thermal shear tensor) [57] of strange quarks in the coalescence model. The goal of this paper is to fill this gap by providing a more rigorous estimation of the effects of hydrodynamic gradients to the spin alignment of vector mesons in heavy ion collisions. This will provide a baseline for more exotic mechanisms such as the fluctuating background fields stemming from the strong interaction [67–71,78–80] (see also Refs. [84–86] for related studies in proton-proton and proton-nucleus collisions and jet polarization).

In this paper, starting with the Wigner function of vector mesons and its expansion up to the second order in $\hbar$, equivalent to second order space-time gradients, we derive an expression for the 00-component of the spin density matrix (ρ_{00}) in terms of the distribution functions of vector mesons, for which the primary results are shown in Eqs. (50)–(52). We further discuss the high momentum and low momentum limits of ρ_{00} as shown in Eqs. (55) and (60), respectively. In order to quantitatively estimate the order of magnitude of ρ_{00} from such contributions, we adopt a thermal model with single-freeze-out [87] to evaluate ρ_{00} for ϕ and $K^{*0}-$mesons.

The paper is structured as follows. In Sec. II, we derive the Wigner functions of polarized vector mesons up to order $\hbar^2$. In Sec. III, we derive a new equation for the ρ_{00}-component of the spin density matrix in terms of the gradients of vector meson distributions and provide simplified expressions in the high and low momentum limits. In Sec. IV, we outline the main steps involved in the calculation of various experimental observables related to spin alignments of vector meson using the thermal model with single freeze-out. In Sec. V, we discuss our numerical results. In Sec. VI, we present a summary of this work and an outlook. Some technical details are provided in the Appendices.

Notation and conventions: Throughout this paper the mostly minus signature of the Minkowski metric $\eta^{\mu\nu} = \mathrm{diag}(1,-1,-1,-1)$ is used. The notations $A^{(\mu}B^{\nu)} \equiv A^\mu B^\nu + A^\nu B^\mu$ and $A^{[\mu}B^{\nu]} \equiv A^\mu B^\nu - A^\nu B^\mu$ are employed to define symmetric and antisymmetric tensors respectively. Greek letters (μ, ν etc) are used for space and time components (indices take on values 0,1,2,3) while Latin letters i, j etc stand for spatial components (taking on values 1,2,3).

II. WIGNER FUNCTIONS OF VECTOR MESONS

The spin-1 vector-meson field can be expanded as [75],

$$V^\mu(x) = \sum_{\lambda=\pm1,0} \int \frac{d^3k}{(2\pi)^3\sqrt{2E_k}} [\epsilon^\mu(\lambda,k)a(\lambda,\boldsymbol{k})e^{-ik\cdot x} + \epsilon^{*\mu}(\lambda,k)b^\dagger(\lambda,\boldsymbol{k})e^{ik\cdot x}], \tag{1}$$

where $k \equiv (E_k, \boldsymbol{k})$ is the on-shell four-momentum with $E_k = \sqrt{|\boldsymbol{k}|^2 + M^2}$ being the energy, $\boldsymbol{k}$ the momentum and M the mass of the considered vector meson. $a^\dagger(\lambda,\boldsymbol{k})$ and $a(\lambda,\boldsymbol{k})$ are the creation and annihilation operators for particles while $b^\dagger(\lambda,\boldsymbol{k})$ and $b(\lambda,\boldsymbol{k})$ are those for antiparticles, which follow the respective mesonic commutation relations. In principle, for interacting vector mesons, there could be further corrections to the wave functions beyond the simple plane waves in the above mode expansion. For our consideration, we focus on the simplest case by ignoring such corrections and instead absorbing the interaction-dependent corrections into the creation and annihilation operators or more precisely the distribution functions, in which the interaction dependence is dictated by the kinetic equation after the Wigner transformation. The four vector $\epsilon^\mu(\lambda,k)$ is the polarization vector. Following Refs. [75,79], it can for a vector meson be written as

$$\epsilon^\mu(\lambda,k) = \left(\frac{-k_\alpha \epsilon^\alpha_{\lambda,\perp}}{M}, \epsilon^\mu_{\lambda,\perp} - \frac{k_\alpha \epsilon^\alpha_{\lambda,\perp}}{M(E_q+M)} k^\mu_\perp\right), \tag{2}$$

where $V^\mu_\perp = \Delta^{\mu\nu}V_\nu$ with $\Delta^{\mu\nu} = \eta^{\mu\nu} - n^\mu n^\nu$ and $n^\mu = (1,\boldsymbol{0})$. The four-vector $\boldsymbol{\epsilon}^\alpha_{\lambda,\perp} \equiv (\epsilon^0_{\lambda,\perp}, \boldsymbol{\epsilon}^i_{\lambda,\perp})$ satisfies the condition $\epsilon^0_{\lambda,\perp} = 0$ and reduces to $(0,\boldsymbol{\epsilon}_\lambda)$. The three vector $\boldsymbol{\epsilon}_\lambda$ is the spin-state vector, which depends on the spin quantization axis and satisfies the following relation

$$\boldsymbol{\epsilon}_\lambda \cdot \boldsymbol{\epsilon}^*_{\lambda'} = \delta_{\lambda\lambda'}. \tag{3}$$

It can be shown that $\epsilon^\mu(\lambda,k)$ and $\epsilon^*_\mu(\lambda',k)$ satisfy

$$\epsilon^\mu(\lambda,k)\epsilon^*_\mu(\lambda',k) = -\boldsymbol{\epsilon}_\lambda \cdot \boldsymbol{\epsilon}^*_{\lambda'} = -\delta_{\lambda\lambda'}, \tag{4}$$

and

$$\epsilon^\mu(\lambda,k)k_\mu = 0. \tag{5}$$

In the vector meson rest frame, we have $\epsilon^\mu(\lambda,0) = (0,\boldsymbol{\epsilon}_\lambda)$.

The Wigner function for vector mesons in phase space can be written as [88]

$$
\begin{aligned}
W^{<\mu\nu}(q,X) &= \int d^4Y e^{iq\cdot Y}\langle V^{\dagger\nu}(X-Y/2)V^{\mu}(X+Y/2)\rangle \\
&= \pi \sum_{\lambda,\lambda'=\pm1,0}\int \frac{d^3k_-}{(2\pi)^3}\frac{e^{-ik_-\cdot X}}{\left[\left(|\boldsymbol{q}|^2+\frac{|\boldsymbol{k}_-|^2}{4}\right)^2-(\boldsymbol{q}\cdot\boldsymbol{k}_-)^2+2M^2\left(|\boldsymbol{q}|^2+\frac{|\boldsymbol{k}_-|^2}{4}\right)+M^4\right]^{1/4}} \\
&\times\left[\epsilon^{\mu}\left(\lambda,q+\frac{k_-}{2}\right)\epsilon^{*\nu}\left(\lambda',q-\frac{k_-}{2}\right)\left\langle a^{\dagger}\left(\lambda',\boldsymbol{q}-\frac{\boldsymbol{k}_-}{2}\right)a\left(\lambda,\boldsymbol{q}+\frac{\boldsymbol{k}_-}{2}\right)\right\rangle\delta(q^0-k_+^0)\right. \\
&\left.+\epsilon^{\nu}\left(\lambda',-q+\frac{k_-}{2}\right)\epsilon^{*\mu}\left(\lambda,-q-\frac{k_-}{2}\right)\left\langle b\left(\lambda',-\boldsymbol{q}+\frac{\boldsymbol{k}_-}{2}\right)b^{\dagger}\left(\lambda,-\boldsymbol{q}-\frac{\boldsymbol{k}_-}{2}\right)\right\rangle\delta(q^0+k_+^0)\right],
\end{aligned}
\tag{6}
$$

where

$$
k_+^0=\frac{1}{2}\left(E_{q+\frac{k_-}{2}}+E_{q-\frac{k_-}{2}}\right),\qquad k_-^0=\left(E_{q+\frac{k_-}{2}}-E_{q-\frac{k_-}{2}}\right).
\tag{7}
$$

For ϕ mesons, $a(\lambda,\boldsymbol{k})=b(\lambda,\boldsymbol{k})$. In order to carry out the integration over k_-, we expand the integrand for small k_- and keep the terms up to $\mathcal{O}(k_-^2)$, which corresponds to the $\hbar$ expansion up to $\mathcal{O}(\hbar^2)$. Thus,

$$
\begin{aligned}
k_+^0=\frac{1}{2}\left(E_{q+\frac{k_-}{2}}+E_{q-\frac{k_-}{2}}\right) &\approx (M^2+|\boldsymbol{q}|^2)^{1/2}+\frac{(M^2+|\boldsymbol{q}|^2)|\boldsymbol{k}_-|^2-(\boldsymbol{q}\cdot k_-)^2}{8(M^2+|\boldsymbol{q}|^2)^{3/2}}+O(|\boldsymbol{k}_-|^3) \\
&= E_q+\Delta E_q,
\end{aligned}
\tag{8}
$$

where $\Delta E_q=\frac{E_q^2|\boldsymbol{k}_-|^2-(\boldsymbol{q}\cdot\boldsymbol{k}_-)^2}{8E_q^3}$. Furthermore,

$$
\begin{aligned}
\delta(q^0-k_+^0) &= \delta(q_0-E_q-\Delta E_q) \\
&= 2(E_q+\Delta E_q)\delta(q^2-M^2-2E_q\Delta E_q) \\
&\approx 2E_q\delta(q^2-M^2)+2\Delta E_q\delta(q^2-M^2)-4E_q^2\Delta E_q\delta'(q^2-M^2),
\end{aligned}
\tag{9}
$$

and

$$
\begin{aligned}
\left[\left(|\boldsymbol{q}|^2+\frac{|\boldsymbol{k}_-|^2}{4}\right)^2-(\boldsymbol{q}\cdot\boldsymbol{k}_-)^2+2M^2\left(|\boldsymbol{q}|^2+\frac{|\boldsymbol{k}_-|^2}{4}\right)+M^4\right]^{-1/4} &\approx \frac{1}{(|\boldsymbol{q}|^2+M^2)^{1/2}}+\frac{(-M^2-|\boldsymbol{q}|^2+2|\boldsymbol{q}|^2\cos[\theta]^2)|\boldsymbol{k}_-|^2}{8(|\boldsymbol{q}|^2+M^2)^{5/2}} \\
&= \frac{1}{E_q}\left[1-\frac{\Delta E_q}{E_q}+\frac{(\boldsymbol{q}\cdot\boldsymbol{k}_-)^2}{8E_q^4}\right].
\end{aligned}
\tag{10}
$$

We shall consider only the presence of diagonal spin components by postulating

$$
\left\langle a^{\dagger}\left(\lambda',\boldsymbol{q}-\frac{\boldsymbol{k}_-}{2}\right)a\left(\lambda,\boldsymbol{q}+\frac{\boldsymbol{k}_-}{2}\right)\right\rangle\propto\delta_{\lambda\lambda'}
\tag{11}
$$

and similarly for antiparticles. Now, the polarization-related structure appearing in the Wigner function can be approximated as

$$
\epsilon_{\mu}\left(\lambda,q+\frac{k_-}{2}\right)\epsilon_{\nu}^{*}\left(\lambda,q-\frac{k_-}{2}\right)\approx\Pi_{\mu\nu}^{(0)}(\lambda,q)+\frac{k_-^{\alpha}}{2}\Pi_{\mu\nu\alpha}^{(1)}(\lambda,q)+\frac{1}{2!}\frac{k_-^{\alpha}}{2}\frac{k_-^{\beta}}{2}\Pi_{\mu\nu\alpha\beta}^{(2)}(\lambda,q)
\tag{12}
$$

up to $\mathcal{O}(k_-^2)$, where

$$
\Pi_{\mu\nu}^{(0)}(\lambda,q)\equiv\epsilon_{\mu}(\lambda,q)\epsilon_{\nu}^{*}(\lambda,q),
\tag{13}
$$

$$\Pi^{(1)}_{\mu\nu\alpha}(\lambda,q) \equiv (\partial_{q^\alpha}\epsilon_\mu(\lambda,q))\epsilon^*_\nu(\lambda,q) - \epsilon_\mu(\lambda,q)(\partial_{q^\alpha}\epsilon^*_\nu(\lambda,q)), \tag{14}$$

and

$$\begin{aligned}\Pi^{(2)}_{\mu\nu\alpha\beta}(\lambda,q) \equiv{}& (\partial_{q^\alpha}\partial_{q^\beta}\epsilon_\mu(\lambda,q))\epsilon^*_\nu(\lambda,q) \\ &+ \epsilon_\mu(\lambda,q)(\partial_{q^\alpha}\partial_{q^\beta}\epsilon^*_\nu(\lambda,q)) \\ &- ((\partial_{q^\alpha}\epsilon_\mu(\lambda,q))(\partial_{q^\beta}\epsilon^*_\nu(\lambda,q)) \\ &+ (\partial_{q^\beta}\epsilon_\mu(\lambda,q))(\partial_{q^\alpha}\epsilon^*_\nu(\lambda,q))).\end{aligned} \tag{15}$$

For simplicity, we will hereafter neglect the contribution for antiparticles. That is, we do not show the similar derivation for Wigner functions associated with $\langle b^\dagger b\rangle$. For the ϕ meson, which is its own antiparticle, such a contribution automatically vanishes. The Wigner function for vector mesons accordingly takes the form

$$W^{<\mu\nu}(q,X) = \sum_{\lambda=\pm1,0} W^{<\mu\nu}(\lambda,q,X), \tag{16}$$

where

$$\begin{aligned}W^{<\mu\nu}(\lambda,q,X) = \pi\int\frac{d^3k_-}{(2\pi)^3}e^{-ik_-\cdot X}\frac{1}{E_q}\left[1-\frac{\Delta E_q}{E_q}+\frac{(\boldsymbol{q}\cdot\boldsymbol{k}_-)^2}{8E_q^4}\right]\left[\left(\Pi^{\mu\nu}_{(0)}(\lambda,q)+\frac{k_{-\alpha}}{2}\Pi^{\mu\nu\alpha}_{(1)}(\lambda,q)+\frac{1}{2!}\frac{k_{-\alpha}}{2}\frac{k_{-\beta}}{2}\Pi^{\mu\nu\alpha\beta}_{(2)}(\lambda,q)\right)\right. \\ \left.\times(2(E_q+\Delta E_q)\delta(q^2-M^2)-4E_q^2\Delta E_q\delta'(q^2-M^2))\left\langle a^\dagger\left(\lambda,\boldsymbol{q}-\frac{\boldsymbol{k}_-}{2}\right)a\left(\lambda,\boldsymbol{q}+\frac{\boldsymbol{k}_-}{2}\right)\right\rangle\right].\end{aligned} \tag{17}$$

For our purpose, we are interested in the on-shell Wigner function,

$$W^{<\mu\nu}(\lambda,\boldsymbol{q},X) = \int\frac{dq_0}{(2\pi)}W^{<\mu\nu}(\lambda,q,X), \tag{18}$$

from which we introduce

$$W^{<\mu\nu}(\boldsymbol{q},X) = \sum_{\lambda=\pm1,0} W^{<\mu\nu}(\lambda,\boldsymbol{q},X), \tag{19}$$

for its polarization averaged component. Keeping all the terms up to $\mathcal{O}(\boldsymbol{k}_-^2)$ and carrying out the integration over $\boldsymbol{k}_-$, one arrives at

$$\begin{aligned}W^{<\mu\nu}(\lambda,\boldsymbol{q},X) \sim{}& \frac{1}{2E_q}\left(\Pi^{\mu\nu}_{(0)}(\lambda,q)+\frac{i\hbar}{2}\Pi^{\mu\nu\alpha}_{(1)}\partial_\alpha(\lambda,q)\right. \\ &\left.-\frac{\hbar^2}{8}\Pi^{\mu\nu\alpha\beta}_{(2)}(\lambda,q)\partial_\alpha\partial_\beta\right)\tilde{f}_\lambda(\boldsymbol{q},X),\end{aligned} \tag{20}$$

where we have introduced the polarization dependent distribution functions,

$$\tilde{f}_\lambda(\boldsymbol{q},X) = \left[1+\frac{\hbar^2}{8M^2}\left(\nabla^2-\frac{(q\cdot\nabla)^2}{E_q^2}\left(1+\frac{M^2}{E_q^2}\right)\right)\right]f_\lambda(\boldsymbol{q},X) \tag{21}$$

stemming from the expectation values of number operators

$$f_\lambda(\boldsymbol{q},X) = \int\frac{\mathrm{d}^3k_-}{(2\pi)^3}\mathrm{e}^{-\mathrm{i}k_-\cdot X}\left\langle a^\dagger\left(\lambda,\boldsymbol{q}-\frac{\boldsymbol{k}_-}{2}\right)a\left(\lambda,\boldsymbol{q}+\frac{\boldsymbol{k}_-}{2}\right)\right\rangle. \tag{22}$$

The custom of redefining distribution functions within the $\hbar$ expansion is commonly adopted in the Wigner-function approach for constructing quantum kinetic theories [45,89].

Given our expression of the Wigner function, one may further utilize the Kadanoff-Baym equation in the real-time formalism to derive the quantum kinetic equations for tracking the phase-space evolution of $\tilde{f}_\lambda(\boldsymbol{q},X)$ [55,90]. However, such a derivation would be complicated, with a realistic collision term depending on the details of the interaction. In practice, it is even technically challenging to numerically solve a classical kinetic equation for spin-averaged vector mesons. Instead of seeking a precise value of ρ_{00}, the purpose of this work is to estimate the order of magnitude of the effect that the second order gradients have on ρ_{00}. It will hence here be sufficient to adopt the polarization-averaged distribution function obtained from classical transport equations to calculate ρ_{00} from the Wigner function up to second order gradients as will be discussed in the subsequent sections.

III. SPIN DENSITY MATRIX

Diagonal elements of the spin density matrix are defined by the formula [77]

$$\rho_{\lambda\lambda}(q) = \frac{\int d\Sigma_X\cdot q\epsilon_\mu(\lambda,q)\epsilon^*_\nu(\lambda,q)W^{<\mu\nu}(\boldsymbol{q},X)}{\int d\Sigma_X\cdot q\sum_{\lambda'=\pm1,0}\epsilon_\mu(\lambda',q)\epsilon^*_\nu(\lambda',q)W^{<\mu\nu}(\boldsymbol{q},X)}, \tag{23}$$

where $d\Sigma_{X\mu}$ denotes a freeze-out hyper-surface. The 00-component of the spin density matrix can further be expressed as

$$\rho_{00}(q) = \frac{\int d\Sigma_X \cdot q[\Pi^{(0)}_{\mu\nu}(0,q)W^{<\mu\nu}(\boldsymbol{q},X)]}{\int d\Sigma_X \cdot q[\Pi^{(0)}_{\mu\nu}(0,q)+\Pi^{(0)}_{\mu\nu}(-1,q)+\Pi^{(0)}_{\mu\nu}(+1,q)]W^{<\mu\nu}(\boldsymbol{q},X)}. \tag{24}$$

We can further decompose the Wigner function into symmetric and antisymmetric components,

$$\tilde{W}^{<\mu\nu} = \tilde{W}_S^{<\mu\nu} + i\tilde{W}_A^{<\mu\nu}, \tag{25}$$

where

$$\tilde{W}_S^{<\mu\nu} \equiv \frac{1}{2}(\tilde{W}^{<\mu\nu}+\tilde{W}^{<\nu\mu}), \qquad \tilde{W}_A^{<\mu\nu} \equiv \frac{-i}{2}(\tilde{W}^{<\mu\nu}-\tilde{W}^{<\nu\mu}). \tag{26}$$

Here, $\tilde{W}_S^{<\mu\nu}$ and $\tilde{W}_A^{<\mu\nu}$ are both real functions since $\tilde{W}^{<\mu\nu}$ by definition is Hermitian.

Thus, ρ_{00} can then be written as

$$\rho_{00}(q) = \frac{\int d\Sigma_X \cdot q(\epsilon_{(\mu}(0,q)\epsilon^*_{\nu)}(0,q)W_S^{<\mu\nu}(\boldsymbol{q},X) + i\epsilon_{[\mu}(0,q)\epsilon^*_{\nu]}(0,q)W_A^{<\mu\nu}(\boldsymbol{q},X))}{\int d\Sigma_X \cdot q\sum_{\lambda=\pm1,0}(\epsilon_{(\mu}(\lambda,q)\epsilon^*_{\nu)}(\lambda,q)W_S^{<\mu\nu}(\boldsymbol{q},X) + i\epsilon_{[\mu}(\lambda,q)\epsilon^*_{\nu]}(\lambda,q)W_A^{<\mu\nu}(\boldsymbol{q},X))}. \tag{27}$$

We may next reexpress the distribution functions for $\lambda = \pm1$ in terms of $\tilde{f}_{\pm1} = f_V \pm f_A/2$, where $f_A = \tilde{f}_1 - \tilde{f}_{-1} \neq 0$ characterizes a nonzero spin polarization of vector mesons. When averaging over the spin polarization, we may set $\tilde{f}_\lambda = f_V$ with $f_A = 0$. In principle, as briefly explained in the previous section, we should work out the quantum kinetic equations for each $\tilde{f}_\lambda$ with $\hbar$ corrections in the presence of collisions. $\tilde{W}^{\mu\nu}(\lambda,q,X)$ may furthermore possibly involve $\hbar$ corrections pertinent to interactions. However, for simplicity, we here only consider the quantum correction induced by the spacetime-derivative terms in Eq. (20) obtained in the collisionless limit and incorporate collisional effects in $\tilde{f}_\lambda(q,X)$ only from polarization-averaged transport theory. Consequently, we will simply consider the case of $\tilde{f}_\lambda = f_V$ and vanishing $W_A^{\mu\nu}$ at $\mathcal{O}(\hbar^0)$.

Note that the essential source of spin alignment considered in this work is led by $\partial_\alpha f_V$ and $\partial_\alpha\partial_\beta f_V$. Since ρ_{00} is a normalized quantity, an overall factor of the Wigner function should not matter. To obtain a more concrete expression of ρ_{00}, we shall further compute the coefficients associated with the momentum derivatives on the polarization vectors explicitly.

A. Decomposition of $\Pi^{\mu\nu}_{(0)}(\lambda,q)$, $\Pi^{\mu\nu\alpha}_{(1)}(\lambda,q)$ and $\Pi^{\mu\nu\alpha\beta}_{(2)}(\lambda,q)$ in symmetric and antisymmetric parts

We first decompose $\Pi^{\mu\nu}_{(0)}$ in symmetric and antisymmetric components such that $\Pi^{\mu\nu}_{(0)}(\lambda,q) = \frac{1}{2}(\Pi^{(\mu\nu)}_{(0)}(\lambda,q) + \Pi^{[\mu\nu]}_{(0)}(\lambda,q))$ where

$$\Pi^{(\mu\nu)}_{(0)}(\lambda,q) \equiv \epsilon^{(\mu}(\lambda,q)\epsilon^{*\nu)}(\lambda,q), \tag{28}$$

and

$$\Pi^{[\mu\nu]}_{(0)}(\lambda,q) \equiv \epsilon^{[\mu}(\lambda,q)\epsilon^{*\nu]}(\lambda,q). \tag{29}$$

Similarly, $\Pi^{(1)}_{\mu\nu\alpha}(\lambda,q)$ and $\Pi^{(2)}_{\mu\nu\alpha\beta}(\lambda,q)$ can be decomposed in symmetric and antisymmetric parts as

$$\Pi^{[\mu\nu]\alpha}_{(1)}(\lambda,q) = (\partial^\alpha_q\epsilon^{[\mu}(\lambda,q))\epsilon^{*\nu]}(\lambda,q) + \text{c.c.}, \tag{30}$$

$$\Pi^{(\mu\nu)\alpha}_{(1)}(\lambda,q) = (\partial^\alpha_q\epsilon^{(\mu}(\lambda,q))\epsilon^{*\nu)}(\lambda,q) - \text{c.c.}, \tag{31}$$

$$\Pi^{[\mu\nu]\alpha\beta}_{(2)}(\lambda,q) \equiv \Big((\partial^\alpha_q\partial^\beta_q\epsilon^{[\mu}(\lambda,q))\epsilon^{*\nu]}(\lambda,q) - ((\partial^\alpha_q\epsilon^{[\mu}(\lambda,q))(\partial^\beta_q\epsilon^{*\nu]}(\lambda,q)))\Big) - \text{c.c.}, \tag{32}$$

$$\Pi^{(\mu\nu)\alpha\beta}_{(2)}(\lambda,q) \equiv \Big((\partial^\alpha_q\partial^\beta_q\epsilon^{(\mu}(\lambda,q))\epsilon^{*\nu)}(\lambda,q) - ((\partial^\alpha_q\epsilon^{(\mu}(\lambda,q))(\partial^\beta_q\epsilon^{*\nu)}(\lambda,q)))\Big) + \text{c.c.}, \tag{33}$$

where c.c. represents the complex conjugate. We choose the y direction as the spin quantization axis, in which case the corresponding spin state vectors read [75]

$$\boldsymbol{\epsilon}_0 = (0,1,0), \tag{34}$$

$$\boldsymbol{\epsilon}_{+1} = -\frac{1}{\sqrt{2}}(i,0,1), \tag{35}$$

$$\boldsymbol{\epsilon}_{-1} = \frac{1}{\sqrt{2}}(-i,0,1), \tag{36}$$

which satisfy the relation

$$\sum_{\lambda=\pm1,0} \boldsymbol{\epsilon}_\lambda^m \boldsymbol{\epsilon}_\lambda^{*n} = \delta^{mn}. \tag{37}$$

Using Eqs. (34)–(36), one can show that the polarization tensor ϵ^μ [see Eq. (2)] satisfies

$$\epsilon^\mu(0,q) = \epsilon^{*\mu}(0,q), \tag{38}$$

$$\epsilon^\mu(1,q) = -\epsilon^{*\mu}(-1,q). \tag{39}$$

Based on the above properties, we have

$$\Pi_{(0)}^{(\mu\nu)}(1,q) = \Pi_{(0)}^{(\mu\nu)}(-1,q), \tag{40}$$

$$\Pi_{(0)}^{[\mu\nu]}(1,q) = -\Pi_{(0)}^{[\mu\nu]}(-1,q), \tag{41}$$

and

$$\begin{aligned}\Pi_{(1)}^{(\mu\nu)\alpha}(1,q) &= (\partial_q^\alpha \epsilon^{(\mu}(1,q))\epsilon^{*\nu)}(1,q) - \text{c.c.} \\ &= -\Pi_{(1)}^{(\mu\nu)\alpha}(-1,q),\end{aligned} \tag{42}$$

$$\Pi_{(1)}^{[\mu\nu]\alpha}(1,q) = (\partial_q^\alpha \epsilon^{[\mu}(1,q))\epsilon^{*\nu]}(1,q) + \text{c.c.} = \Pi_{(1)}^{[\mu\nu]\alpha}(-1,q), \tag{43}$$

$$\begin{aligned}\Pi_{(2)}^{(\mu\nu)\alpha\beta}(1,q) &\equiv \Big((\partial_q^\alpha\partial_q^\beta \epsilon^{(\mu}(1,q))\epsilon^{*\nu)}(1,q) \\ &\quad - ((\partial_q^\alpha \epsilon^{(\mu}(1,q))(\partial_q^\beta \epsilon^{*\nu)}(1,q)))\Big) + \text{c.c.} \\ &= \Pi_{(2)}^{(\mu\nu)\alpha\beta}(-1,q),\end{aligned} \tag{44}$$

$$\begin{aligned}\Pi_{(2)}^{[\mu\nu]\alpha\beta}(1,q) &\equiv \Big((\partial_q^\alpha\partial_q^\beta \epsilon^{[\mu}(1,q))\epsilon^{*\nu]}(1,q) \\ &\quad - ((\partial_q^\alpha \epsilon^{[\mu}(1,q))(\partial_q^\beta \epsilon^{*\nu]}(1,q)))\Big) - \text{c.c.} \\ &= -\Pi_{(2)}^{[\mu\nu]\alpha\beta}(-1,q).\end{aligned} \tag{45}$$

Moreover, using Eq. (38), we can show that

$$\Pi_{(0)}^{[\mu\nu]}(0,q) = 0, \tag{46}$$

$$\Pi_{(1)}^{(\mu\nu)\alpha}(0,q) = 0, \tag{47}$$

$$\Pi_{(2)}^{[\mu\nu]\alpha\beta}(0,q) = 0. \tag{48}$$

Making use of Eqs. (40)–(48) for Eq. (20) and substituting $\tilde{f}_{0,\pm1} = f_V$, we obtain

$$\begin{aligned}W^{<\mu\nu}(q,X) = \frac{1}{2E_q}\Big[&\frac{1}{2}\Pi_{(0)}^{(\mu\nu)}(q) + \frac{i\hbar}{4}(\Pi_{(1)}^{[\mu\nu]\alpha}(1,q) + \Pi_{(1)}^{[\mu\nu]\alpha}(-1,q) + \Pi_{(1)}^{[\mu\nu]\alpha}(0,q))\partial_\alpha \\ &- \frac{\hbar^2}{16}(\Pi_{(2)}^{(\mu\nu)\alpha\beta}(1,q) + \Pi_{(2)}^{(\mu\nu)\alpha\beta}(-1,q) + \Pi_{(2)}^{(\mu\nu)\alpha\beta}(0,q))\partial_\alpha\partial_\beta\Big] f_V(q,X),\end{aligned} \tag{49}$$

where $\Pi_{(0)}^{(\mu\nu)}(q) = \sum_{\lambda=\pm1,0}\Pi_{(0)}^{(\mu\nu)}(\lambda,q) = 2(\frac{q^\mu q^\nu}{M^2} - \eta^{\mu\nu})$.

Eventually, ρ_{00} reads

$$\rho_{00}(q) = \frac{\int d\Sigma_X \cdot q\left[1 - \frac{\hbar^2}{32}\Pi_{(\mu\nu)}^{(0)}(0,q)\Pi_{(2)}^{(\mu\nu)\alpha\beta}(q)\partial_\alpha\partial_\beta\right] f_V(q,X)}{\int d\Sigma_X \cdot q\left[3 - \frac{\hbar^2}{32}\Pi_{(\mu\nu)}^{(0)}(q)\Pi_{(2)}^{(\mu\nu)\alpha\beta}(q)\partial_\alpha\partial_\beta\right] f_V(q,X)}, \tag{50}$$

where $\Pi_{(\mu\nu)}^{(0)}(0,q)\Pi_{(2)}^{(\mu\nu)\alpha\beta}(q)\partial_\alpha\partial_\beta$ and $\Pi_{(\mu\nu)}^{(0)}(q)\Pi_{(2)}^{(\mu\nu)\alpha\beta}(q)\partial_\alpha\partial_\beta$, can be written as

$$\begin{aligned}\Pi_{(\mu\nu)}^{(0)}(0,q)\Pi_{(2)}^{(\mu\nu)\alpha\beta}(q)\partial_\alpha\partial_\beta = &\left[\frac{2(q^y)^2}{M^2}A_1 - \frac{4(q^y)^2E_q}{M^2}B_2\right]\partial_\alpha\partial^\alpha + (4(B_3+C_3)E_q - 4(A_2+C_2)) \\ &\times\left[\frac{q^y}{M}\left(\partial^y + \frac{q^y(q^i\partial^i)}{M(E_q+M)}\right)\right]q^\alpha\partial_\alpha + \left[\frac{4(q^yE_q)^2}{M^2}E_3 - \frac{4(q^y)^2}{M}\frac{E_q}{M}D_2\right](q^\alpha\partial_\alpha)^2 \\ &+ 4A_3\left[(\partial^y)^2 + \frac{2q^y}{M(E_q+M)}(q^i\partial^i)\partial^y + \frac{(q^y)^2}{M^2(E_q+M)^2}(q^i\partial^i)^2\right]\end{aligned} \tag{51}$$

and

$$\Pi^{(0)}_{(\mu\nu)}(q)\Pi^{(\mu\nu)\alpha\beta}_{(2)}(q)\partial_\alpha\partial_\beta = 2\Bigg[\left(\left(\frac{E_q^2}{M^2}-1\right)A_1 - \frac{2|\boldsymbol{q}|^2}{M^2}E_qB_2\right)\partial_\alpha\partial^\alpha + 2A_3(\partial^i\partial^i) + \frac{2}{M^2}A_3(q^i\partial^i)^2 + \frac{E_q}{M^2}(2E_q(B_3+C_3) - 2(A_2+C_2))(q^i\partial^i)(q^\beta\partial_\beta) + E_q\left(\frac{|\boldsymbol{q}|^2}{M^2}\right)(2E_qE_3 - 2D_2)(q^\beta\partial_\beta)^2\Bigg]. \quad (52)$$

The coefficients A_{1-3}, B_{2-3}, C_{2-3}, D_2, and E_3 are listed in Appendix B. We shall in the next section examine the large-momentum and low-momentum limits, in which ρ_{00} assumes a greatly simplified form.

B. Large-momentum limit

At large momentum, $|\boldsymbol{q}| \gg M$ and we have $E_q \sim |\boldsymbol{q}|$, which leads to

$$\Pi^{(0)}_{(\mu\nu)}(0,q)\Pi^{(\mu\nu)\alpha\beta}_{(2)}(q)\partial_\alpha\partial_\beta \approx -\frac{4(q^y)^2}{M^4|\boldsymbol{q}|^2}\Big[3|\boldsymbol{q}|^2(\partial_t)^2 - |\boldsymbol{q}|^2(\partial^i)^2 - 4(q^i\partial^i)q^\alpha\partial_\alpha\Big], \quad (53)$$

and

$$\Pi^{(0)}_{(\mu\nu)}(q)\Pi^{(\mu\nu)\alpha\beta}_{(2)}(q)\partial_\alpha\partial_\beta \approx -\left(\frac{4}{M^4}\right)\Big[3|\boldsymbol{q}|^2(\partial_t)^2 - |\boldsymbol{q}|^2(\partial^i)^2 - 4(q^i\partial^i)q^\alpha\partial_\alpha\Big]. \quad (54)$$

Using Eqs. (53) and (54), we can simplify Eq. (50) to

$$\rho_{00}(q) = \frac{\int d\Sigma_X\cdot q\left[1+\frac{\hbar^2}{8}\frac{(q^y)^2}{M^4}\boxtimes\right]f_V(q,X)}{\int d\Sigma_X\cdot q\left[3+\frac{\hbar^2}{8}\left(\frac{|\boldsymbol{q}|^2}{M^4}\right)\boxtimes\right]f_V(q,X)}, \quad (55)$$

where

$$\boxtimes = \left(3(\partial_t)^2 - (\partial^i)^2 - \frac{4}{|\boldsymbol{q}|^2}(q^i\partial^i)q^\alpha\partial_\alpha\right). \quad (56)$$

The above result shows that $\rho_{00} - 1/3$ at large momentum could be substantially enhanced when $\mathcal{O}(|\boldsymbol{q}|^2\partial^2 f_V/(M^4 f_V)) \sim \mathcal{O}(1)$.

C. Small-momentum limit

In the small momentum limit, $|\boldsymbol{q}| \ll M$, we have $E_q \sim M$, giving

$$\Pi^{(0)}_{(\mu\nu)}(0,q)\Pi^{(\mu\nu)\alpha\beta}_{(2)}(q)\partial_\alpha\partial_\beta \approx 4A_3(\partial^y)^2 = 2(\partial^y)^2/M^2, \quad (57)$$

and

$$\Pi^{(0)}_{(\mu\nu)}(q)\Pi^{(\mu\nu)\alpha\beta}_{(2)}(q)\partial_\alpha\partial_\beta \approx 4A_3(\partial^i)^2 = 2(\partial^i)^2/M^2. \quad (58)$$

Thus, $\rho_{00}(q)$ for this case becomes

$$\rho_{00}(q) = \frac{\int d\Sigma_X\cdot q\left[1-\frac{\hbar^2}{4}\frac{(\partial^y)^2}{M^2}\right]f_V(q,X)}{\int d\Sigma_X\cdot q\left[3-\frac{\hbar^2}{4}\frac{(\partial^i)^2}{M^2}\right]f_V(q,X)}, \quad (59)$$

which can be further approximated as

$$\rho_{00}(q) = \frac{1}{3} - \frac{\hbar^2}{12M^2}\frac{\int d\Sigma_X\cdot q(2(\partial^y)^2 - (\partial^x)^2 - (\partial^z)^2)f_V(q,X)}{\int d\Sigma_X\cdot q f_V(q,X)}, \quad (60)$$

when $\mathcal{O}(\partial^2 f_V/(M^2 f_V)) \ll 1$.

IV. SPIN ALIGNMENT OBSERVABLES WITHIN A THERMAL MODEL WITH SINGLE FREEZE OUT

In order to estimate ρ_{00}, we assume the vector mesons to follow the Jüttner distribution, ($f_V(q,X) = \exp[-q^\mu\beta_\mu(x) - \xi(x)]$ where, $\beta^\mu = u^\mu/T$ and $\xi = \mu/T$ are ratios of the four fluid velocity and the chemical potential to the temperature) and use a thermal model with single-freeze-out [87] which has been used in the past to describe various features of soft hadron production (particle yields, transverse-momentum spectra, elliptic flow, HBT radii) for Au + Au collisions at the top RHIC energies ($\sqrt{s_{NN}} = 130$ GeV) [91–95]. In its standard formulation, it uses two thermodynamic parameters (temperature T, baryon chemical potential μ_B) and two geometric parameters (proper time τ_f and system size $r_{\max}$) which characterize the freeze-out hypersurface (defined through the conditions: $\tau_f^2 = t^2 - x^2 - y^2 - z^2$ and $x^2 + y^2 \le r_{\max}^2$) and hydrodynamic flow (which is assumed to have a Hubble-like form, $u^\mu = x^\mu/\tau$). The thermodynamic parameters T, μ_B are obtained by fitting the ratios of hadronic abundances to experimental data while the geometric ones (τ_f and $r_{\max}$) are determined by fits to experimental transverse-momentum spectra. In this work, we use the extended thermal model with a single freeze out, in which phenomena such as elliptic flow are included by taking into account the elliptic deformations of both the emission region in the transverse plane and the transverse flow [96] in terms of two new parameters ϵ and δ. To include the elliptical asymmetry in the transverse plane, the transverse region is modeled by the parametrization

TABLE I. Values of the parameters previously used to describe the PHENIX data at $\sqrt{s_{NN}} = 130$ GeV for different centrality classes [97,98]. The freeze-out temperature used in the calculation is $T_f = 165$ MeV.

c%	ϵ	δ	τ_f [fm]	$r_{\max}$ [fm]
0–15	0.055	0.12	7.666	6.540
15–30	0.097	0.26	6.258	5.417
30–60	0.137	0.37	4.266	3.779

$$x = r_{\max}\sqrt{1-\epsilon}\cos\phi,$$
$$y = r_{\max}\sqrt{1+\epsilon}\sin\phi, \tag{61}$$

where ϕ is the azimuthal angle, while $r_{\max}$ and ϵ are the model parameters. $\epsilon > 0$ indicates that the system formed in the collision is elongated in the y direction.

Flow asymmetry is included by parametrizing the flow velocity as

$$u^\mu = \frac{1}{N}(t, x\sqrt{1+\delta}, y\sqrt{1-\delta}, z), \tag{62}$$

where the parameter δ characterizes the anisotropy of the transverse flow. $\delta > 0$, indicates that there is more flow in the reaction plane (elliptic flow). The constant N can be obtained from the normalization condition $u^\mu u_\mu = 1$, yielding

$$N = \sqrt{\tau^2 - (x^2 - y^2)\delta}, \tag{63}$$

where the proper time τ is given by

$$\tau^2 = t^2 - x^2 - y^2 - z^2. \tag{64}$$

The adopted parameter values for ϵ, δ, τ_f, and $r_{\max}$ are listed in Table I. These values have been used in the past to describe the PHENIX data for the centrality classes $c = 0$–15%, $c = 15\%$–30% and $c = 30\%$–60% at beam energy $\sqrt{s_{NN}} = 130$ GeV and freeze-out temperature $T_f = 0.165$ GeV [97,98]. We furthermore assume that the freeze-out takes place at a constant value of the proper time, i.e., at $\tau = \tau_f$. In this case, the element of the freeze-out hypersurface, $d\Sigma_{X\lambda}$, can be expressed as

$$d\Sigma_{X\lambda} = n_\lambda dx dy d\eta, \tag{65}$$

where

$$n^\lambda = \left(\sqrt{\tau_f^2 + x^2 + y^2}\cosh\eta, x, y, \sqrt{\tau_f^2 + x^2 + y^2}\sinh\eta\right), \tag{66}$$

with $n^\lambda n_\lambda = \tau_f^2$ and $\eta = \frac{1}{2}\ln[(t+z)/(t-z)]$ being the space-time rapidity.

The particle four momentum reads

$$q^\mu = (E_q, q_x, q_y, q_z) = (m_T\cosh y_p, q_x, q_y, m_T\sinh y_p), \tag{67}$$

where $m_T = \sqrt{m^2 + q_T^2}$ is the transverse mass, $q_T = \sqrt{q_x^2 + q_y^2}$ and m being the transverse momentum and mass of the particle, respectively. $y_p = \frac{1}{2}\ln[(E_q + q_z)/(E_q - q_z)]$ is the particle rapidity. Using Eqs. (62) and (67) we can write,

$$q^\mu\beta_\mu = R_1\cosh(y_p - \eta) + R_2, \tag{68}$$

where

$$R_1 = \frac{m_T(\cosh(y_p)t - \sinh(y_p)z)}{T_f\sqrt{t^2 - x^2 - y^2 - z^2 - (x^2 - y^2)\delta}}, \tag{69}$$

$$R_2 = -\frac{(x\sqrt{1+\delta}q_x + y\sqrt{1-\delta}q_y)}{T_f\sqrt{t^2 - x^2 - y^2 - z^2 - (x^2 - y^2)\delta}}. \tag{70}$$

Accordingly, we have

$$d\Sigma_X \cdot q = (G_1\cosh(y_p - \eta) + G_2)dx\,dy\,d\eta, \tag{71}$$

where

$$G_1 = m_T\sqrt{\tau_f^2 + x^2 + y^2}, \tag{72}$$

$$G_2 = -(xq_x + yq_y). \tag{73}$$

At the top RHIC energies we can neglect effects of the baryon number density and calculate the contribution from temperature gradients using the hydrodynamic equations within the perfect fluid approximation (see Appendix A of Ref. [99] for details). In such a situation, using Eqs. (51) and (52), we can easily carry out the freeze-out integration in (50) and plot $\delta\rho_{00}(q_x, q_y) = \rho_{00}(q_x, q_y) - \frac{1}{3}$ as a function of q_x and q_y. The azimuthal angle dependence $\rho_{00}(\phi_p)$ (at fixed particle rapidity $y_p = 0$) can be obtained by taking the momentum average of $\rho_{00}(q)$ weighted by the momentum spectrum of the considered meson [73,80],

$$\langle\rho_{00}(\phi_q)\rangle = \frac{\int q_T dq_T[\rho_{00}(\mathbf{q})\mathcal{N}]}{\int dq_T q_T\mathcal{N}}, \tag{74}$$

where $\mathcal{N} = \int d\Sigma_X \cdot q f_V(q, X)$. One can also look at ρ_{00} as a function of q_T at $y_p = 0$. In this case, we perform the azimuthal-angle integrals in both the numerator and

denominator, keeping the transverse momentum fixed, namely

$$\langle \rho_{00}(q_T) \rangle = \frac{\int d\phi_p [\rho_{00}(\mathbf{q}) \mathcal{N}]}{\int d\phi_p \mathcal{N}}. \tag{75}$$

Finally, one can also obtain the rapidity dependence of ρ_{00} from the formula

$$\langle \rho_{00}(y_p) \rangle = \frac{\int q_T dq_T \int d\phi_p [\rho_{00}(\mathbf{q}) \mathcal{N}]}{\int q_T dq_T \int d\phi_p \mathcal{N}}. \tag{76}$$

V. RESULTS AND DISCUSSIONS

In this section we present the numerical results for ϕ and K^{*0} mesons, making use of the thermal model parameters of Table I.

In Fig. 1, we show the contour plot of $\delta\rho_{00}$ for K^{*0} (left panel from top to bottom) and ϕ (right panel from top to bottom) as a function of q_x and q_y for the three centrality classes $c = 0$–15%, $c = 15\%$–30%, and $c = 30\%$–60% at $y_p = 0$. For K^{*0} mesons we observe a significant quadrupole structure for $\delta\rho_{00}$ which changes sign as a function of q_x and q_y. At smaller q_x, q_y (in the domain $q_x \in (-1.5, 1.5)$ GeV and $q_y \in (-1.5, 1.5)$ GeV) when $|q_y| \gg |q_x|$ we have $\delta\rho_{00} < 0$ while for $|q_y| \ll |q_x|$ such that $0.5 < |q_x| < 1.5$ we have $\delta\rho_{00} > 0$. On the other hand, at higher momentum ($|q_x|, |q_y| > 1.5$ GeV) when $|q_x| \gg |q_y|$, we see $\delta\rho_{00} < 0$ while for $|q_y| \gg |q_x|$, $\delta\rho_{00} > 0$. A similar pattern for the ϕ meson with slightly different ranges of q_x and q_y is observed. We note that, albeit the complicated structures, the difference in the results for K^{*0} and ϕ interestingly only stem from their mass difference.

In Fig. 2, we present the numerical results for the azimuthal angle (ϕ_q) (left panel) and the transverse momentum (q_T) dependence (right panel) of ρ_{00} as defined in Eqs. (74) and (75) for K^{*0} and ϕ. The azimuthal angle dependence is obtained by integrating over q_T in the range 1.2–5.4 GeV. The corresponding plots indicate that $\langle \rho_{00}(\phi_q) \rangle$ can be accurately parametrized as $\langle \rho_{00}(\phi_q) \rangle = a \cos(2\phi_q) + b$ with $b \simeq 1/3$, while $a < 0$ for K^{*0} and $a > 0$ for ϕ. Our estimate for the values of the coefficients a and b obtained by fitting the above defined function $\langle \rho_{00}(\phi_q) \rangle$ to the numerical data for three different centrality classes are listed in the Table II. Such values can be probed in future RHIC and LHC experiments. The sign change of a for K^{*0} and ϕ might be inferred from their dependence on $q_{x,y}$ for $\delta\rho_{00}$. As shown in Fig. 1, for $q_y = 0$ and equivalently $\phi_q = 0$, one finds that $\delta\rho_{00}$ is mostly negative for K^{*0} despite being positive in a marginal region for $\bar{q}_x \sim 0$, where $\bar{q}_x = |q_x| - 1.2$ GeV, while for ϕ, $\delta\rho_{00}$ is mostly positive in a larger region around $\bar{q}_x \sim 0$, which is more prominently weighted compared to the large-$\bar{q}_x$ region. When integrating over q_T (more precisely $\bar{q}_x$), it turns out that $\delta\rho_{00}$ at $\phi_q = 0$ may thus become negative and positive for K^{*0} and ϕ, respectively. Analogously, one finds the opposite patterns for $\phi_q = \pi/2$. We hence observe the opposite oscillatory pattern of $\langle \rho_{00}(\phi_q) \rangle$ for K^{*0} and ϕ. Since $\mathcal{N}$ is suppressed by larger m, the overall deviation of $\langle \rho_{00}(\phi_q) \rangle$ from $1/3$ (if nonzero) is more prominent for K^{*0} as shown in Fig. 2. Overall, our finding shows that the azimuthal-angle dependence of ρ_{00} is rather sensitive to the mass values of the considered vector mesons.

Our results of $\langle \rho_{00}(q_T) \rangle$ for K^{*0} and ϕ indicate that in different momentum ranges the values to ρ_{00} can be $\leq 1/3$ as well as $\geq 1/3$. At small transverse momentum ($q_T < 1.7$ GeV) one notices that for both particles ρ_{00} is roughly $1/3$ for all the three centrality classes. At higher momenta of the order of $q_T \sim 4$ GeV, ρ_{00} can be larger than $1/3$ for the lowest centrality class of $c = 0$–15%, but decreases considerably below $1/3$ with increasing q_T for higher centralities.

In Fig. 3, we depict the rapidity dependence of ρ_{00} for K^{*0} and ϕ. In the case of K^{*0}, one notes that ρ_{00} decreases with increasing rapidity y_p and centrality c. In contrast, ρ_{00} for the ϕ initially increases with respect to y_p then decreases rapidly below $1/3$ at larger y_p for all centrality classes with more prominent decrease at higher centrality. Since ρ_{00} for the ϕ is close to $1/3$ in the region of $|y_p| \lesssim 1$, it can be expected that its global value by further integrating over y_p is also close to $1/3$. For the global spin alignment of K^{*0}, the deviation from $1/3$ may be larger than that of ϕ, but still rather small.

VI. SUMMARY AND OUTLOOK

In this paper, expanding the Wigner function of vector mesons up to $O(\hbar^2)$, we have derived an expression for ρ_{00} in terms of their distribution functions. We further discussed the large-momentum and small-momentum limits of ρ_{00}. As a result, we find that the second-order space-time gradients of the vector-meson distribution functions can trigger spin alignment, leading to a deviation of ρ_{00} from $1/3$. Next, by considering the Jüttner type equilibrium distribution and using a thermal model with single freeze-out, we computed several spin alignment observables for Au-Au collisions with $\sqrt{s_{NN}} = 130$ GeV. Studying the dependence of ρ_{00} on the azimuthal angle ϕ_q at midrapidity, we found a $\langle \rho_{00}(\phi_q) \rangle = a \cos(2\phi_q) + b$ pattern, with $b \simeq 1/3$ for both K^{*0} and ϕ, but $a < 0$ for K^{*0} and $a > 0$ for ϕ. For $\langle \rho_{00}(q_T) \rangle$ at midrapidity, our results indicate that the deviations of ρ_{00} from $1/3$ could be greatly enhanced at large transverse momenta for different collision centralities. We furthermore studied the rapidity dependence of ρ_{00} for K^{*0} and ϕ at different centralities, obtaining a rather different behavior for the two particles, as shown in

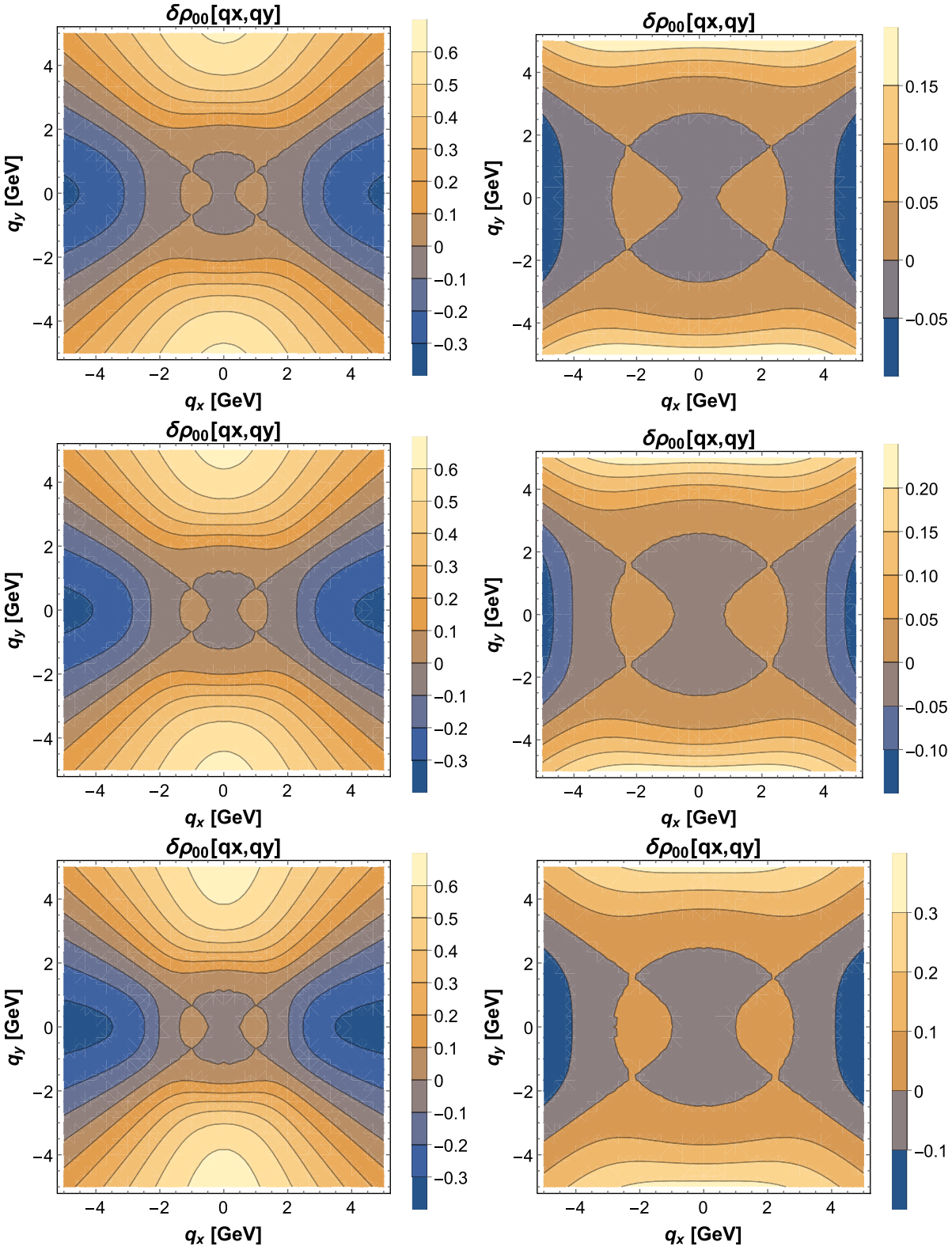

FIG. 1. The contour plots of $\delta\rho_{00} = \rho_{00} - 1/3$ as a function of q_x and q_y for K^{*0} (left panels) and the ϕ meson (right panels) for the centrality classes $c = 0$–15%, $c = 15\%$–30% and $c = 30\% - 60\%$ (top to bottom) with freeze-out temperature $T_f = 165$ MeV and collision energy $\sqrt{s_{NN}} = 130$ GeV at $y_p = 0$.

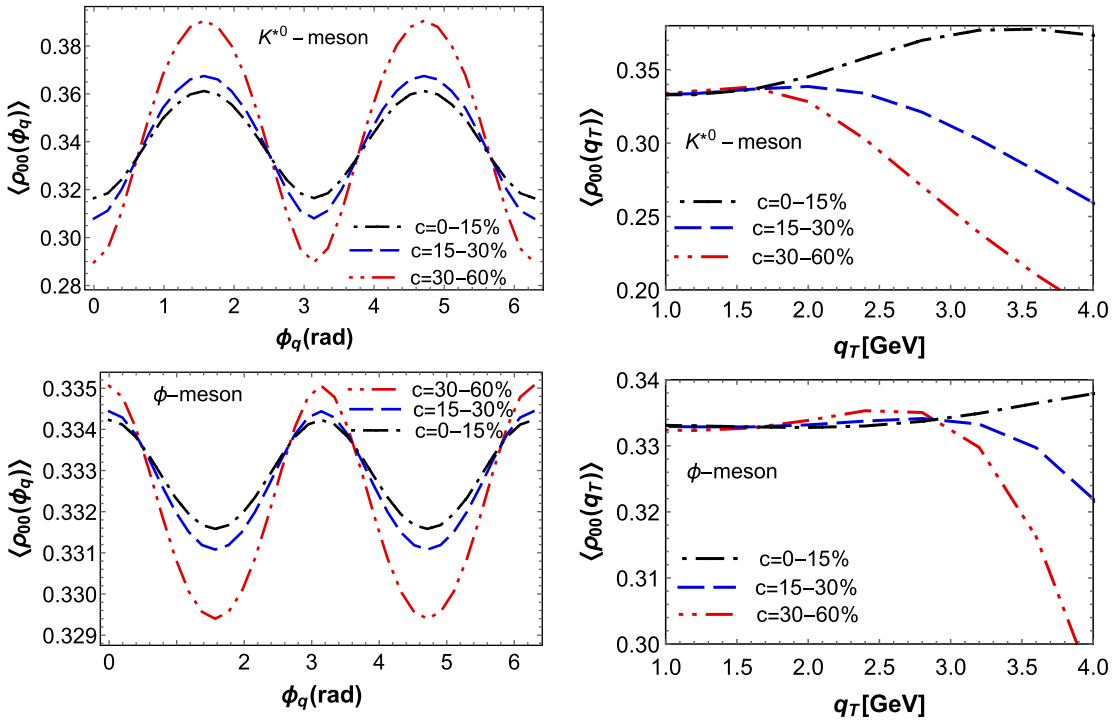

FIG. 2. Azimuthal angle (left panel) and transverse momentum dependence (right panel) of the ρ_{00} component of the spin density matrix for K^{*0} (upper panels) and ϕ mesons (lower panels) for the centrality classes $c = 0$–15%, $c = 15$–30%, and $c = 30$–60% with freeze-out temperature $T_f = 165$ MeV and collision energy $\sqrt{s_{NN}} = 130$ GeV at $y_p = 0$.

TABLE II. Values of the coefficients a and b obtained by fitting the function $\langle\rho_{00}(\phi_q)\rangle = a\cos(2\phi_q) + b$ to our numerical data for different centrality classes.

c%	a (K^{*0}–meson)	a (ϕ–meson)	b (K^{*0}–meson)	b (ϕ–meson)
0–15	−0.0223	0.0013	0.3399	0.3329
15–30	−0.0295	0.0017	0.3406	0.3327
30–60	−0.0498	0.0028	0.3453	0.3321

Fig. 3. For more accurate and versatile estimates, that go beyond the simple model used in this work, we will in the future conduct hydrodynamic simulations with broader ranges of collision energies.

As mentioned in the discussion of our setup in Sec. II, we have neglected dynamical contributions to ρ_{00} from the polarization dependent $\tilde{f}_\lambda(\boldsymbol{q}, X)$. For example, early-time effects could exist, which lead to further $\mathcal{O}(\hbar^2)$ corrections to $\tilde{f}_\lambda(\boldsymbol{q}, X)$, such as glasma fields [78,79], turbulent color

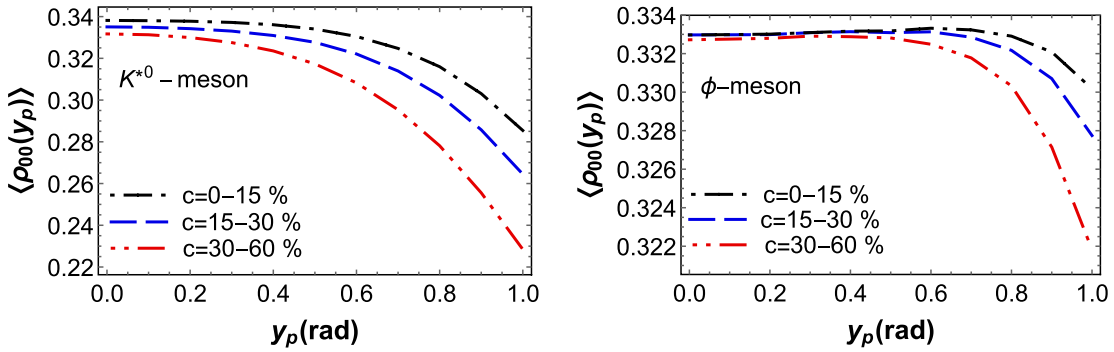

FIG. 3. Rapidity dependence of the ρ_{00} component of the spin density matrix for K^{*0} (left panel) and ϕ mesons (right panel) for the centrality classes $c = 0$–15%, $c = 15\%$–30%, and $c = 30\%$–60% with freeze-out temperature $T_f = 165$ MeV and collision energy $\sqrt{s_{NN}} = 130$ GeV.

fields in the QGP phase [70,71], and fluctuating meson fields before hadronization [67,68,80], which interact with the constituent quark and antiquark forming the vector meson in the quark coalescence scenario [100,101]. In addition, in the hadron phase, polarization dependent interactions could further modify $\tilde{f}_\lambda(\boldsymbol{q}, X)$, which have to be treated within the quantum kinetic theory of vector-mesons with proper collision terms as noted in Sec. II. All these dynamical contributions should be combined with the nondynamical contribution led by the second-order gradients upon $\tilde{f}_\lambda(\boldsymbol{q}, X)$ with a proper choice of the freeze-out hypersurface found in this work to address experimental observations.

On the other hand, since the effect we considered is only related to the final state of vector-meson distribution functions, it is independent of detailed mechanisms for hadronization such as the quark coalescence or fragmentation. As a result, Eq. (50) is applicable to all types of vector mesons with arbitrary momenta and not subject to just K^{*0} and ϕ. In the future, given $\tilde{f}_\lambda(\boldsymbol{q}, X)$ at certain freeze-out points obtained from prescribed transport models, it will become possible to study this effect for J/ψ and D^{*+} at the LHC or K^{*0} and ϕ in low-energy nuclear collisions.

ACKNOWLEDGMENTS

D. Y. was supported in part by the National Science and Technology Council (Taiwan) under Grant No. MOST 110-2112-M-001-070-MY3. P. G. is supported by KAKENHI under Contract No. JP20K03940, No. JP20K03959 and No. JP22H00122.

APPENDIX A: DIFFERENT COMPONENTS OF $\Pi^{(\mu\nu)}(\mathbf{0},\boldsymbol{q}) = \epsilon^{(\mu}(\mathbf{0},\boldsymbol{q})\epsilon^{*\nu)}(\mathbf{0},\boldsymbol{q})$

We start by writing Eq. (2) as

$$\epsilon^\mu(\lambda, q) = \left(\frac{-q_\alpha \epsilon^\alpha_{\lambda,\perp}}{M}, \epsilon^\mu_{\lambda,\perp} - \frac{q_\alpha \epsilon^\alpha_{\lambda,\perp}}{M(E_q + M)} q^\mu_\perp\right). \tag{A1}$$

The spin vectors $\boldsymbol{\epsilon}^i_{\lambda,\perp} = \boldsymbol{\epsilon}^i_\lambda$ appearing in the above equation are given by Eqs. (34)–(36) and satisfy the condition Eq. (37) and $\epsilon^0_{\lambda,\perp} = 0$.

Using Eq. (A1) along with Eq. (34) one obtains

$$\Pi^{(00)}(0, q) = \epsilon^{(0}(0, q)\epsilon^{*0)}(0, q) = \frac{2(q^y)^2}{M^2} \tag{A2}$$

Similarly, using Eq. (A1) with Eqs. (34)–(36) on finds

$$\Pi^{(0i)}(0, q) = \epsilon^{(0}(0, q)\epsilon^{*i)}(0, q) = \frac{2\boldsymbol{q}^y}{M}\left(\epsilon^i_0 + \frac{q^y \boldsymbol{q}^i}{M(E_q + M)}\right), \tag{A3}$$

and

$$\Pi^{(ij)}(0, q) = \epsilon^{(i}(0, q)\epsilon^{*j)}(0, q) = 2\boldsymbol{\epsilon}^i_0 \boldsymbol{\epsilon}^j_0 + \frac{2q^y(q^i \boldsymbol{\epsilon}^j_0 + q^j \boldsymbol{\epsilon}^i_0)}{M(E_q + M)} + \frac{2(q^y)^2 q^i q^j}{M^2(E_q + M)^2}. \tag{A4}$$

APPENDIX B: DIFFERENT COMPONENTS OF $\Pi^{(\mu\nu)\alpha\beta}_{(2)}(\boldsymbol{q})$

The tensor, $\Pi^{(\mu\nu)\alpha\beta}_{(2)}(q)$ is defined as

$$\Pi^{(\mu\nu)\alpha\beta}_{(2)}(\lambda, q) \equiv ((\partial^\alpha_q \partial^\beta_q \epsilon^{(\mu}(\lambda, q))\epsilon^{*\nu)}(\lambda, q) - ((\partial^\alpha_q \epsilon^{(\mu}(\lambda, q))(\partial^\beta_q \epsilon^{*\nu)}(\lambda, q)))) + \text{c.c.} \tag{B1}$$

Using Eq. (A1) on can easily show

$$\Pi^{(00)\alpha\beta}_{(2)}(q) = A_1 \eta^{\alpha\beta}, \tag{B2}$$

with

$$A_1 = \frac{2}{M^2}, \tag{B3}$$

where the factor 2 comes from the complex conjugate.

Now, using Eqs. (37) and (A1) one can write

$$\Pi^{(0i)\alpha\beta}_{(2)}(q) = A_2 \eta^{\alpha i} q^\beta + B_2 \eta^{\alpha\beta} q^i + C_2 q^\alpha \eta^{\beta i} + D_2 q^\alpha q^i q^\beta, \tag{B4}$$

where

$$\begin{aligned}
A_2 &= -2\frac{1}{M^2(E_q + M)}\left(1 + \frac{|q|^2}{E_q(E_q + M)}\right) = -\frac{2(2E_q - M)}{M^2 E_q(E_q + M)}, \\
B_2 &= 2\frac{1}{M^2(E_q + M)}\left(2 - \frac{|q|^2}{E_q(E_q + M)}\right) = +\frac{2}{M^2 E_q}, \\
C_2 &= \frac{2}{M^2(E_q + M)}, \\
D_2 &= 2\frac{1}{M^2 E_q(E_q + M)^2}\left(\frac{(3E_q + M)|q|^2}{E_q^2(E_q + M)}\right) = \frac{2(3E_q + M)(E_q - M)}{M^2 E_q^3(E_q + M)^2}.
\end{aligned} \tag{B5}$$

Similarly, one can write

$$\Pi^{(ij)\alpha\beta}_{(2)}(q) = [A_3\eta^{\alpha(i}\eta^{\beta j)} + B_3 q^{(i}\eta^{\beta j)}q^{\alpha} + C_3 q^{(i}\eta^{\alpha j)}q^{\beta} + D_3\eta^{\alpha\beta}q^{(i}q^{j)} + E_3 q^{\alpha}q^{\beta}q^{(i}q^{j)}], \tag{B6}$$

where

$$\begin{aligned}
A_3 &= 2\frac{1}{M(E_q+M)}\left(2-\frac{|\boldsymbol{q}|^2}{M(E_q+M)}\right) = 2\frac{1}{M(E_q+M)}\left(3-\frac{E_q}{M}\right),\\
B_3 &= -2\frac{1}{ME_q(E_q+M)^2}\left(1-\frac{|\boldsymbol{q}|^2}{M(E_q+M)}\right) = -2\frac{1}{ME_q(E_q+M)^2}\left(2-\frac{E_q}{M}\right),\\
C_3 &= -2\frac{1}{M(E_q+M)^2}\left(\frac{2}{E_q}\right),\\
D_3 &= 2\frac{1}{M(E_q+M)^2}\left(\frac{1}{M}-\frac{1}{E_q}\left(1+\frac{|\boldsymbol{q}|^2}{M(E_q+M)}\right)\right) = 0,\\
E_3 &= 2\frac{1}{ME_q(E_q+M)^3}\left(\frac{(3E_q+M)}{E_q^2}+\frac{1}{M}\left(2+\frac{(3E_q+M)|\boldsymbol{q}|^2}{E_q^2(E_q+M)}\right)-\frac{1}{M}\left(2+\frac{|\boldsymbol{q}|^2}{E_q(E_q+M)}\right)\right)\\
&= \frac{4}{M^2E_q^2(E_q+M)^2}.
\end{aligned} \tag{B7}$$

[1] Z.-T. Liang and X.-N. Wang, Spin alignment of vector mesons in noncentral A + A collisions, Phys. Lett. B **629**, 20 (2005).

[2] S. A. Voloshin, Polarized secondary particles in unpolarized high energy hadron-hadron collisions?, arXiv:nucl-th/0410089.

[3] S. A. Voloshin, Vorticity and particle polarization in heavy ion collisions (experimental perspective), EPJ Web Conf. **171**, 07002 (2018).

[4] Z.-T. Liang and X.-N. Wang, Globally polarized quark-gluon plasma in noncentral A + A collisions, Phys. Rev. Lett. **94**, 102301 (2005); **96**, 039901(E) (2006).

[5] B. Betz, M. Gyulassy, and G. Torrieri, Polarization probes of vorticity in heavy ion collisions, Phys. Rev. C **76**, 044901 (2007).

[6] F. Becattini, F. Piccinini, and J. Rizzo, Angular momentum conservation in heavy ion collisions at very high energy, Phys. Rev. C **77**, 024906 (2008).

[7] J.-H. Gao, S.-W. Chen, W.-t. Deng, Z.-T. Liang, Q. Wang, and X.-N. Wang, Global quark polarization in non-central A + A collisions, Phys. Rev. C **77**, 044902 (2008).

[8] S. J. Barnett, Magnetization by rotation, Phys. Rev. **6**, 239 (1915).

[9] S. J. Barnett, Gyromagnetic and electron-inertia effects, Rev. Mod. Phys. **17**, 129 (1935).

[10] STAR Collaboration, Global Λ hyperon polarization in nuclear collisions: Evidence for the most vortical fluid, Nature (London) **548**, 62 (2017).

[11] J. Adam *et al.* (STAR Collaboration), Polarization of Λ ($\bar{\Lambda}$) hyperons along the beam direction in Au + Au collisions at $\sqrt{s_{NN}} = 200$ GeV, Phys. Rev. Lett. **123**, 132301 (2019).

[12] J. Adam *et al.* (STAR Collaboration), Global polarization of Λ hyperons in Au + Au collisions at $\sqrt{s_{NN}} = 200$ GeV, Phys. Rev. C **98**, 014910 (2018).

[13] J. Adam *et al.* (STAR Collaboration), Global polarization of Ξ and Ω hyperons in Au + Au collisions at $\sqrt{s_{NN}} = 200$ GeV, Phys. Rev. Lett. **126**, 162301 (2021).

[14] S. Acharya *et al.* (ALICE Collaboration), Global polarization of $\Lambda\bar{\Lambda}$ hyperons in Pb-Pb collisions at $\sqrt{s_{NN}} = 2.76$ and 5.02 TeV, Phys. Rev. C **101**, 044611 (2020).

[15] F. J. Kornas (HADES Collaboration), Λ polarization in Au + Au collisions at $\sqrt{s_{NN}} = 2.4$ GeV measured with HADES, Springer Proc. Phys. **250**, 435 (2020).

[16] F. Becattini, V. Chandra, L. Del Zanna, and E. Grossi, Relativistic distribution function for particles with spin at local thermodynamical equilibrium, Ann. Phys. (Amsterdam) **338**, 32 (2013).

[17] F. Becattini, I. Karpenko, M. Lisa, I. Upsal, and S. Voloshin, Global hyperon polarization at local thermodynamic

equilibrium with vorticity, magnetic field and feed-down, Phys. Rev. C **95**, 054902 (2017).
[18] I. Karpenko and F. Becattini, Study of Λ polarization in relativistic nuclear collisions at $\sqrt{s_{\rm NN}} = 7.7$–200 GeV, Eur. Phys. J. C **77**, 213 (2017).
[19] F. Becattini and I. Karpenko, Collective longitudinal polarization in relativistic heavy-ion collisions at very high energy, Phys. Rev. Lett. **120**, 012302 (2018).
[20] R.-h. Fang, L.-g. Pang, Q. Wang, and X.-n. Wang, Polarization of massive fermions in a vortical fluid, Phys. Rev. C **94**, 024904 (2016).
[21] Y. Xie, D. Wang, and L. P. Csernai, Global Λ polarization in high energy collisions, Phys. Rev. C **95**, 031901 (2017).
[22] L.-G. Pang, H. Petersen, Q. Wang, and X.-N. Wang, Vortical fluid and Λ spin correlations in high-energy heavy-ion collisions, Phys. Rev. Lett. **117**, 192301 (2016).
[23] H. Li, L.-G. Pang, Q. Wang, and X.-L. Xia, Global Λ polarization in heavy-ion collisions from a transport model, Phys. Rev. C **96**, 054908 (2017).
[24] D.-X. Wei, W.-T. Deng, and X.-G. Huang, Thermal vorticity and spin polarization in heavy-ion collisions, Phys. Rev. C **99**, 014905 (2019).
[25] S. Ryu, V. Jupic, and C. Shen, Probing early-time longitudinal dynamics with the Λ hyperon's spin polarization in relativistic heavy-ion collisions, Phys. Rev. C **104**, 054908 (2021).
[26] X.-L. Xia, H. Li, Z.-B. Tang, and Q. Wang, Probing vorticity structure in heavy-ion collisions by local Λ polarization, Phys. Rev. C **98**, 024905 (2018).
[27] Y. Hidaka, S. Pu, and D.-L. Yang, Nonlinear responses of chiral fluids from kinetic theory, Phys. Rev. D **97**, 016004 (2018).
[28] S. Y. F. Liu and Y. Yin, Spin Hall effect in heavy-ion collisions, Phys. Rev. D **104**, 054043 (2021).
[29] S. Y. F. Liu and Y. Yin, Spin polarization induced by the hydrodynamic gradients, J. High Energy Phys. 07 (2021) 188.
[30] F. Becattini, M. Buzzegoli, and A. Palermo, Spin-thermal shear coupling in a relativistic fluid, Phys. Lett. B **820**, 136519 (2021).
[31] C. Yi, S. Pu, and D.-L. Yang, Reexamination of local spin polarization beyond global equilibrium in relativistic heavy ion collisions, Phys. Rev. C **104**, 064901 (2021).
[32] Y. Hidaka and D.-L. Yang, Nonequilibrium chiral magnetic/vortical effects in viscous fluids, Phys. Rev. D **98**, 016012 (2018).
[33] D.-L. Yang, Side-jump induced spin-orbit interaction of chiral fluids from kinetic theory, Phys. Rev. D **98**, 076019 (2018).
[34] S. Shi, C. Gale, and S. Jeon, From chiral kinetic theory to relativistic viscous spin hydrodynamics, Phys. Rev. C **103**, 044906 (2021).
[35] M. Buzzegoli, Pseudogauge dependence of the spin polarization and of the axial vortical effect, Phys. Rev. C **105**, 044907 (2022).
[36] S. Fang, S. Pu, and D.-L. Yang, Quantum kinetic theory for dynamical spin polarization from QED-type interaction, Phys. Rev. D **106**, 016002 (2022).
[37] Z. Wang, Spin evolution of massive fermion in QED plasma, Phys. Rev. D **106**, 076011 (2022).
[38] S. Lin and Z. Wang, Shear induced polarization: Collisional contributions, J. High Energy Phys. 12 (2022) 030.
[39] N. Weickgenannt, D. Wagner, E. Speranza, and D. H. Rischke, Relativistic second-order dissipative spin hydrodynamics from the method of moments, Phys. Rev. D **106**, 096014 (2022).
[40] N. Weickgenannt, D. Wagner, E. Speranza, and D. H. Rischke, Relativistic dissipative spin hydrodynamics from kinetic theory with a nonlocal collision term, Phys. Rev. D **106**, L091901 (2022).
[41] S. Bhadury, W. Florkowski, A. Jaiswal, A. Kumar, and R. Ryblewski, Relativistic dissipative spin dynamics in the relaxation time approximation, Phys. Lett. B **814**, 136096 (2021).
[42] S. Bhadury, W. Florkowski, A. Jaiswal, A. Kumar, and R. Ryblewski, Dissipative spin dynamics in relativistic matter, Phys. Rev. D **103**, 014030 (2021).
[43] M. Buzzegoli, D. E. Kharzeev, Y.-C. Liu, S. Shi, S. A. Voloshin, and H.-U. Yee, Shear-induced anomalous transport and charge asymmetry of triangular flow in heavy-ion collisions, Phys. Rev. C **106**, L051902 (2022).
[44] S. Bhadury, W. Florkowski, A. Jaiswal, A. Kumar, and R. Ryblewski, Relativistic spin magnetohydrodynamics, Phys. Rev. Lett. **129**, 192301 (2022).
[45] Y. Hidaka, S. Pu, and D.-L. Yang, Relativistic chiral kinetic theory from quantum field theories, Phys. Rev. D **95**, 091901 (2017).
[46] J.-H. Gao and Z.-T. Liang, Relativistic quantum kinetic theory for massive fermions and spin effects, Phys. Rev. D **100**, 056021 (2019).
[47] N. Weickgenannt, X.-L. Sheng, E. Speranza, Q. Wang, and D. H. Rischke, Kinetic theory for massive spin-1/2 particles from the Wigner-function formalism, Phys. Rev. D **100**, 056018 (2019).
[48] K. Hattori, Y. Hidaka, and D.-L. Yang, Axial kinetic theory and spin transport for fermions with arbitrary mass, Phys. Rev. D **100**, 096011 (2019).
[49] Z. Wang, X. Guo, S. Shi, and P. Zhuang, Mass correction to chiral kinetic equations, Phys. Rev. D **100**, 014015 (2019).
[50] D.-L. Yang, K. Hattori, and Y. Hidaka, Effective quantum kinetic theory for spin transport of fermions with collisional effects, J. High Energy Phys. 07 (2020) 070.
[51] Z. Wang, X. Guo, and P. Zhuang, Equilibrium spin distribution from detailed balance, Eur. Phys. J. C **81**, 799 (2021).
[52] N. Weickgenannt, E. Speranza, X.-l. Sheng, Q. Wang, and D. H. Rischke, Generating spin polarization from vorticity through nonlocal collisions, Phys. Rev. Lett. **127**, 052301 (2021).
[53] S. Fang, S. Pu, and D.-L. Yang, Spin polarization and spin alignment from quantum kinetic theory with self-energy corrections, arXiv:2311.15197.
[54] F. Becattini, Spin and polarization: A new direction in relativistic heavy ion physics, Rep. Prog. Phys. **85**, 122301 (2022).
[55] Y. Hidaka, S. Pu, Q. Wang, and D.-L. Yang, Foundations and applications of quantum kinetic theory, Prog. Part. Nucl. Phys. **127**, 103989 (2022).

[56] F. Becattini, M. Buzzegoli, G. Inghirami, I. Karpenko, and A. Palermo, Local polarization and isothermal local equilibrium in relativistic heavy ion collisions, Phys. Rev. Lett. **127**, 272302 (2021).
[57] B. Fu, S. Y. F. Liu, L. Pang, H. Song, and Y. Yin, Shear-induced spin polarization in heavy-ion collisions, Phys. Rev. Lett. **127**, 142301 (2021).
[58] W. Florkowski, A. Kumar, A. Mazeliauskas, and R. Ryblewski, Effect of thermal shear on longitudinal spin polarization in a thermal model, Phys. Rev. C **105**, 064901 (2022).
[59] K. Schilling, P. Seyboth, and G. E. Wolf, On the analysis of vector meson production by polarized photons, Nucl. Phys. **B15**, 397 (1970); **B18**, 332(E) (1970).
[60] I. W. Park, H. Sako, K. Aoki, P. Gubler, and S. H. Lee, Disentangling longitudinal and transverse modes of the ϕ meson through dilepton and kaon decays, Phys. Rev. D **107**, 074033 (2023).
[61] S. Acharya *et al.* (ALICE Collaboration), Evidence of spin-orbital angular momentum interactions in relativistic heavy-ion collisions, Phys. Rev. Lett. **125**, 012301 (2020).
[62] S. Acharya *et al.* (ALICE Collaboration), Measurement of the J/ψ polarization with respect to the event plane in Pb-Pb collisions at the LHC, Phys. Rev. Lett. **131**, 042303 (2023).
[63] B. Mohanty, S. Kundu, S. Singha, and R. Singh, Spin alignment measurement of vector mesons produced in high energy collisions, Mod. Phys. Lett. A **36**, 2130026 (2021).
[64] M. S. Abdallah *et al.* (STAR Collaboration), Pattern of global spin alignment of ϕ and K^{*0} mesons in heavy-ion collisions, Nature (London) **614**, 244 (2023).
[65] F. Becattini and F. Piccinini, The ideal relativistic spinning gas: Polarization and spectra, Ann. Phys. (Amsterdam) **323**, 2452 (2008).
[66] Y.-G. Yang, R.-H. Fang, Q. Wang, and X.-N. Wang, Quark coalescence model for polarized vector mesons and baryons, Phys. Rev. C **97**, 034917 (2018).
[67] X.-L. Sheng, L. Oliva, and Q. Wang, What can we learn from the global spin alignment of ϕ mesons in heavy-ion collisions?, Phys. Rev. D **101**, 096005 (2020).
[68] X.-L. Sheng, Q. Wang, and X.-N. Wang, Improved quark coalescence model for spin alignment and polarization of hadrons, Phys. Rev. D **102**, 056013 (2020).
[69] X.-L. Xia, H. Li, X.-G. Huang, and H. Zhong Huang, Local spin alignment of vector mesons in relativistic heavy-ion collisions, Phys. Lett. B **817**, 136325 (2021).
[70] B. Müller and D.-L. Yang, Anomalous spin polarization from turbulent color fields, Phys. Rev. D **105**, L011901 (2022).
[71] D.-L. Yang, Quantum kinetic theory for spin transport of quarks with background chromo-electromagnetic fields, J. High Energy Phys. 06 (2022) 140.
[72] K. J. Goncalves and G. Torrieri, Spin alignment of vector mesons as a probe of spin hydrodynamics and freeze-out, Phys. Rev. C **105**, 034913 (2022).
[73] X.-L. Sheng, L. Oliva, Z.-T. Liang, Q. Wang, and X.-N. Wang, Spin alignment of vector mesons in heavy-ion collisions, Phys. Rev. Lett. **131**, 042304 (2023).
[74] Z. Li, W. Zha, and Z. Tang, Rescattering effect on the measurement of K^{*0} spin alignment in heavy-ion collisions, Phys. Rev. C **106**, 064908 (2022).
[75] X.-L. Sheng, L. Oliva, Z.-T. Liang, Q. Wang, and X.-N. Wang, Relativistic spin dynamics for vector mesons, Phys. Rev. D **109**, 036004 (2024).
[76] F. Li and S. Y. F. Liu, Tensor polarization and spectral properties of vector meson in QCD medium, arXiv:2206.11890.
[77] D. Wagner, N. Weickgenannt, and E. Speranza, Generating tensor polarization from shear stress, Phys. Rev. Res. **5**, 013187 (2023).
[78] A. Kumar, B. Müller, and D.-L. Yang, Spin polarization and correlation of quarks from the glasma, Phys. Rev. D **107**, 076025 (2023).
[79] A. Kumar, B. Müller, and D.-L. Yang, Spin alignment of vector mesons by glasma fields, Phys. Rev. D **108**, 016020 (2023).
[80] X.-L. Sheng, S. Pu, and Q. Wang, Momentum dependence of the spin alignment of the ϕ meson, Phys. Rev. C **108**, 054902 (2023).
[81] P. H. De Moura, K. J. Goncalves, and G. Torrieri, Quarkonium spin alignment in a vortical medium, Phys. Rev. D **108**, 034032 (2023).
[82] Y.-L. Yin, W.-B. Dong, J.-Y. Pang, S. Pu, and Q. Wang, The spin alignment of rho mesons in a pion gas, arXiv:2402.03672.
[83] W.-B. Dong, Y.-L. Yin, X.-L. Sheng, S.-Z. Yang, and Q. Wang, Linear response theory for spin alignment of vector mesons in thermal media, arXiv:2311.18400.
[84] Y.-Q. Ma, T. Stebel, and R. Venugopalan, J/ψ polarization in the CGC + NRQCD approach, J. High Energy Phys. 12 (2018) 057.
[85] T. Stebel and K. Watanabe, J/ψ polarization in high multiplicity pp and pA collisions: CGC + NRQCD approach, Phys. Rev. D **104**, 034004 (2021).
[86] S. Hauksson and E. Iancu, Jet polarisation in an anisotropic medium, J. High Energy Phys. 08 (2023) 027.
[87] W. Broniowski and W. Florkowski, Explanation of the RHIC p(T) spectra in a thermal model with expansion, Phys. Rev. Lett. **87**, 272302 (2001).
[88] K. Hattori, Y. Hidaka, N. Yamamoto, and D.-L. Yang, Wigner functions and quantum kinetic theory of polarized photons, J. High Energy Phys. 02 (2021) 001.
[89] K. Hattori, K. Itakura, and S. Ozaki, Note on all-order Landau-level structures of the Heisenberg-Euler effective actions for QED and QCD, arXiv:2001.06131.
[90] J.-P. Blaizot and E. Iancu, The quark gluon plasma: Collective dynamics and hard thermal loops, Phys. Rep. **359**, 355 (2002).
[91] J. Cleymans and H. Satz, Thermal hadron production in high-energy heavy ion collisions, Z. Phys. C **57**, 135 (1993).
[92] P. Braun-Munzinger, D. Magestro, K. Redlich, and J. Stachel, Hadron production in Au—Au collisions at RHIC, Phys. Lett. B **518**, 41 (2001).
[93] W. Florkowski, W. Broniowski, and M. Michalec, Thermal analysis of particle ratios and p(t) spectra at RHIC, Acta Phys. Pol. B **33**, 761 (2002), https://www.actaphys.uj.edu.pl/R/33/2/761.

[94] F. Becattini, J. Manninen, and M. Gazdzicki, Energy and system size dependence of chemical freeze-out in relativistic nuclear collisions, Phys. Rev. C **73**, 044905 (2006).
[95] A. Andronic, P. Braun-Munzinger, K. Redlich, and J. Stachel, Decoding the phase structure of QCD via particle production at high energy, Nature (London) **561**, 321 (2018).
[96] W. Broniowski, A. Baran, and W. Florkowski, Thermal model at RHIC. Part 2. Elliptic flow and HBT radii, AIP Conf. Proc. **660**, 185 (2003).
[97] A. Baran, Description of azimuthal asymmetry in relativistic heavy-ion collisions based on a thermal model of particle production, Ph.D. thesis (W. Broniowski—supervisor), Institute of Nuclear Physics, Krakow, Poland, 2004.
[98] W. Florkowski, W. Broniowski, and A. Baran, Strange particle production in a single-freeze-out model, J. Phys. G **31**, S1087 (2005).
[99] W. Florkowski, A. Kumar, R. Ryblewski, and A. Mazeliauskas, Longitudinal spin polarization in a thermal model, Phys. Rev. C **100**, 054907 (2019).
[100] R. J. Fries, B. Müller, C. Nonaka, and S. A. Bass, Hadronization in heavy ion collisions: Recombination and fragmentation of partons, Phys. Rev. Lett. **90**, 202303 (2003).
[101] V. Greco, C. M. Ko, and P. Levai, Parton coalescence and antiproton / pion anomaly at RHIC, Phys. Rev. Lett. **90**, 202302 (2003).